

Decoding Holographic Dark Energy in the structure formation

Miguel Sabogal G.¹

Adapted from: W. Cardona and M. A. Sabogal, [arXiv:2210.1333](https://arxiv.org/abs/2210.1333).

¹B.S, Universidad del Atlántico, Colombia

November 15,2022

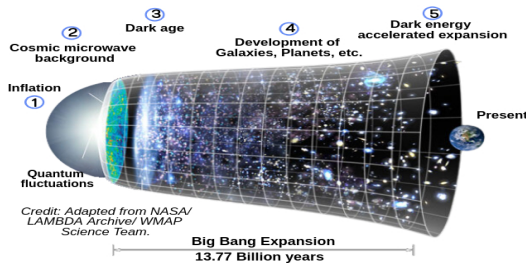
**XIV Latin American Symposium
on High Energy Physics**

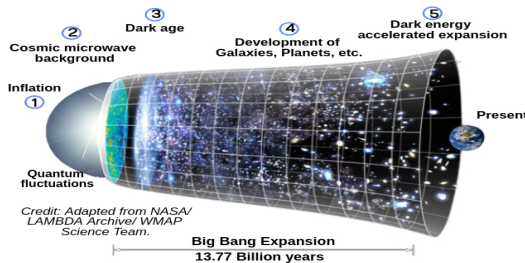
Ecuador, November 14 -18, 2022



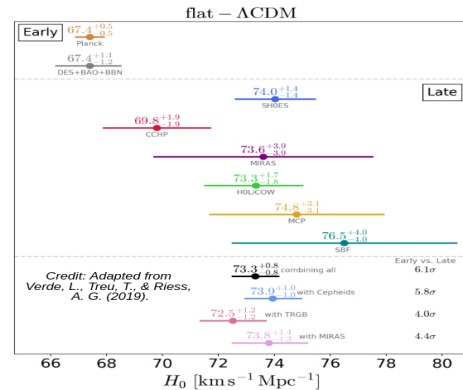
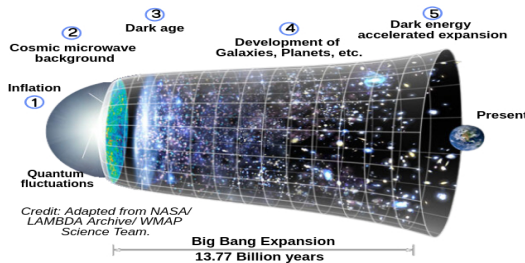
Universidad San Francisco de Quito



 Λ CDM



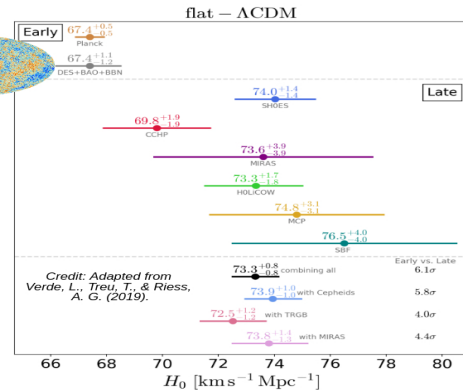
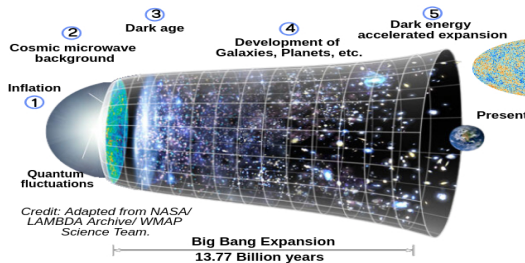
Λ CDM



Fine-tune problem
coincidence problem
 H_0 Tension
 $S8$ Tension



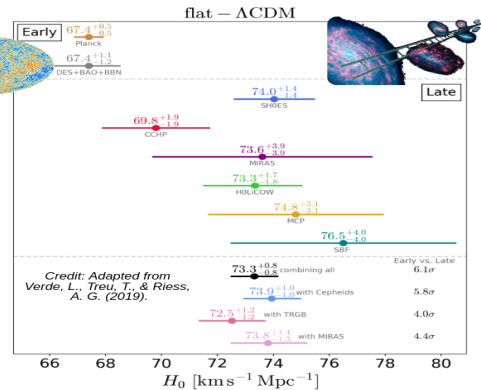
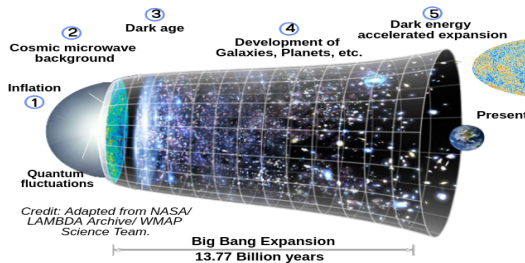
Λ CDM



!

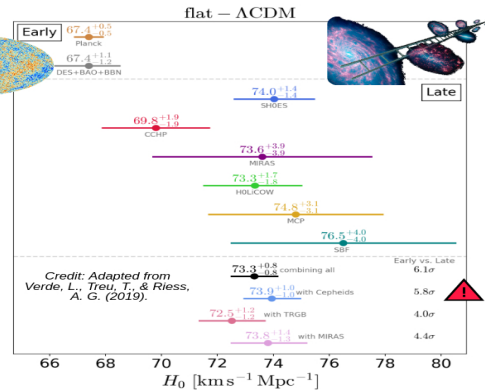
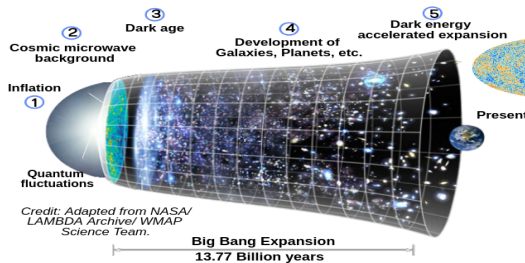
- Fine-tune problem
- coincidence problem
- H_0 Tension
- S8 Tension

Λ CDM



! Fine-tune problem
coincidence problem
 H_0 Tension
 $S8$ Tension

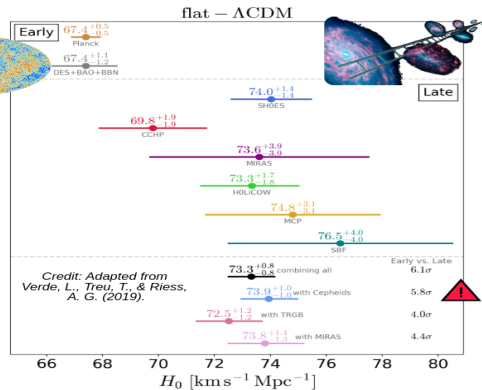
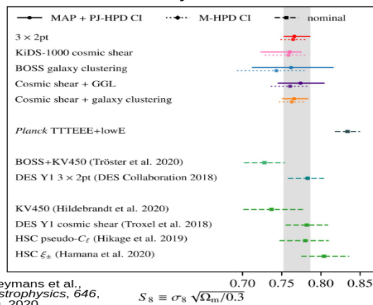
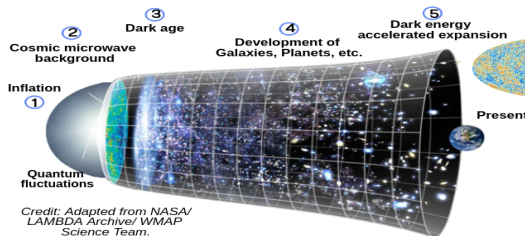
Λ CDM



!

- Fine-tune problem
- coincidence problem
- H_0 Tension
- S8 Tension

Λ CDM

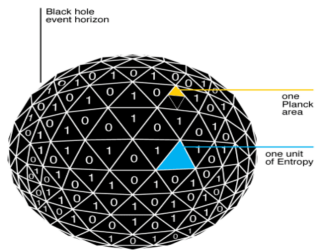


! **Fine-tune problem**
coincidence problem
 H_0 Tension
S8 Tension

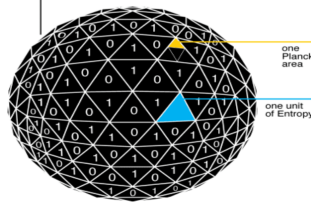
Λ CDM

$$H^2 = \frac{\kappa}{3}(\rho_r + \rho_m + \rho_{de}) \quad (1)$$

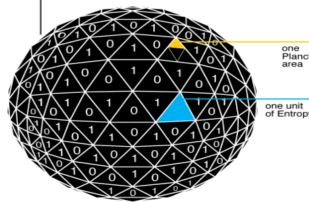
$$H^2 = \frac{\kappa}{3}(\rho_r + \rho_m + \rho_{de}) \quad (1)$$



$$H^2 = \frac{\kappa}{3}(\rho_r + \rho_m + \rho_{de}) \quad (1)$$
$$\rho_{de} = 3\gamma^2 M_p^2 L_{IR}^{-2} \quad (2)$$



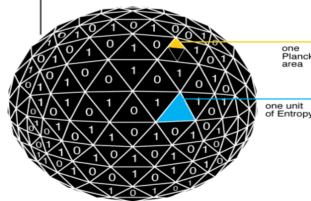
$$H^2 = \frac{\kappa}{3}(\rho_r + \rho_m + \rho_{de}) \quad (1)$$
$$\rho_{de} = 3\gamma^2 M_p^2 L_{IR}^{-2} \quad (2)$$



$$\rho_{de} = \frac{3}{\kappa} \left(\alpha H^2 + \beta \frac{dH}{dt} \right) \quad (3)$$

L.N. Granda & A. Oliveros,
Phys. Lett. B 669, 275–277 (2008)

$$H^2 = \frac{\kappa}{3}(\rho_r + \rho_m + \rho_{de}) \quad (1)$$
$$\rho_{de} = 3\gamma^2 M_p^2 L_{IR}^{-2} \quad (2)$$



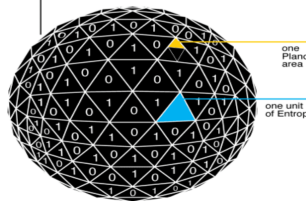
$$\rho_{de} = \frac{3}{\kappa} \left(\alpha H^2 + \beta \frac{dH}{dt} \right) \quad (3)$$

L.N. Granda & A. Oliveros,
Phys. Lett. B 669, 275–277 (2008)

$$\frac{H^2}{H_0^2} = \Omega_{r,0}^{\text{eff}} a^{-4} + \Omega_{m,0}^{\text{eff}} a^{-3} + \Omega_{de,0}^{\text{eff}} a^{\frac{-2(\alpha-1)}{\beta}} \quad (4)$$

$$H^2 = \frac{\kappa}{3}(\rho_r + \rho_m + \rho_{de}) \quad (1)$$

$$\rho_{de} = 3\gamma^2 M_p^2 L_{IR}^{-2} \quad (2)$$



$$\rho_{de} = \frac{3}{\kappa} \left(\alpha H^2 + \beta \frac{dH}{dt} \right) \quad (3)$$

L.N. Granda & A. Oliveros,
Phys. Lett. B 669, 275–277 (2008)

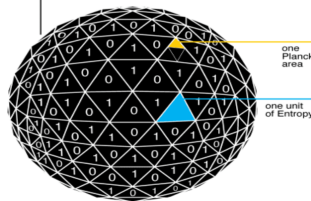
$$\frac{H^2}{H_0^2} = \Omega_{r,0}^{\text{eff}} a^{-4} + \Omega_{m,0}^{\text{eff}} a^{-3} + \Omega_{de,0}^{\text{eff}} a^{\frac{-2(\alpha-1)}{\beta}} \quad (4)$$

$$\begin{aligned} \Omega_{r,0}^{\text{eff}} &\equiv \left(1 + \frac{(\alpha-2\beta)}{(1-\alpha+2\beta)}\right) \Omega_{r,0} \\ \Omega_{m,0}^{\text{eff}} &\equiv \left(1 + \frac{(2\alpha-3\beta)}{(2-2\alpha+3\beta)}\right) \Omega_{m,0} \\ \Omega_{de,0}^{\text{eff}} &\equiv \left(1 - \frac{2\Omega_{m,0}}{(2-2\alpha+3\beta)} - \frac{\Omega_{r,0}}{(1-\alpha+2\beta)}\right) \end{aligned}$$

$$H^2 = \frac{\kappa}{3}(\rho_r + \rho_m + \rho_{de}) \quad (1)$$

$$\rho_{de} = 3\gamma^2 M_p^2 L_{IR}^{-2} \quad (2)$$

$$\rho_{de} = \frac{3}{\kappa} \left(\alpha H^2 + \beta \frac{dH}{dt} \right) \quad (3)$$



L.N. Granda & A. Oliveros,
Phys. Lett. B 669, 275–277 (2008)

$$\frac{H^2}{H_0^2} = \Omega_{r,0}^{\text{eff}} a^{-4} + \Omega_{m,0}^{\text{eff}} a^{-3} + \Omega_{de,0}^{\text{eff}} a^{\frac{-2(\alpha-1)}{\beta}} \quad (4)$$

$$\Omega_{r,0}^{\text{eff}} \equiv \left(1 + \frac{(\alpha-2\beta)}{(1-\alpha+2\beta)}\right) \Omega_{r,0}$$

$$\Omega_{m,0}^{\text{eff}} \equiv \left(1 + \frac{(2\alpha-3\beta)}{(2-2\alpha+3\beta)}\right) \Omega_{m,0}$$

$$\Omega_{de,0}^{\text{eff}} \equiv \left(1 - \frac{2\Omega_{m,0}}{(2-2\alpha+3\beta)} - \frac{\Omega_{r,0}}{(1-\alpha+2\beta)}\right)$$

$$w_{de}(a) = \frac{P_{de}}{\rho_{de}} \quad (5)$$

$$c_a^2(a) = \frac{dP_{de}}{d\rho_{de}} \quad (6)$$

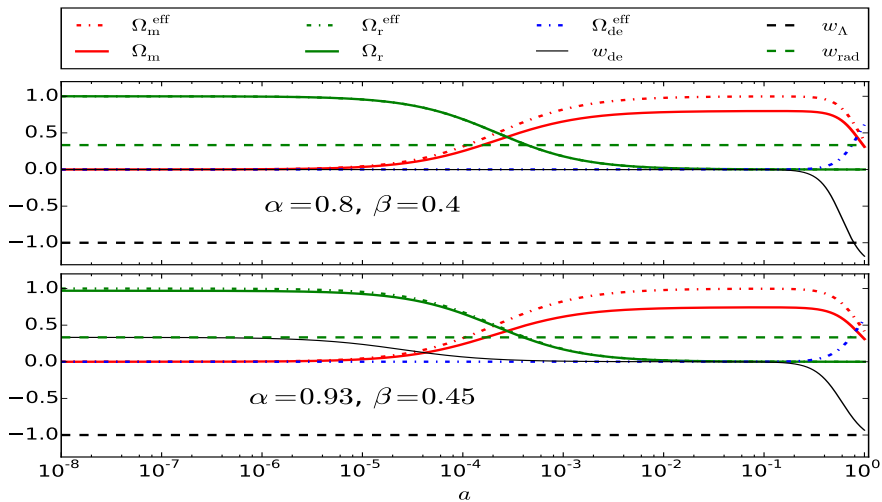


Figure 1: Evolution of parameter densities and HDE equation of state w_{de} for the GO-HDE model. Here we use $\Omega_{m,0} = 0.31$ and $\Omega_{r,0} = 8.5 \times 10^{-5}$.

$$E^2(a) = \Omega_{r,0}a^{-4} + \left(1 + \frac{\alpha}{4-\alpha}\right)\Omega_{m,0}a^{-3} + \left(1 - \frac{\Omega_{m,0}}{1 - \frac{\alpha}{4}} - \Omega_{r,0}\right)a^{\frac{4-4\alpha}{\alpha}} \quad (7)$$

$$w_{de}(a) = \frac{\alpha-4}{3\alpha\left(1 - \frac{\alpha\Omega_{m,0}}{(\alpha-4)(1-\Omega_{r,0})+4\Omega_{m,0}}a^{\frac{\alpha-4}{\alpha}}\right)}$$

$$E^2(a) = \Omega_{r,0}a^{-4} + \left(1 + \frac{\alpha}{4-\alpha}\right)\Omega_{m,0}a^{-3} + \left(1 - \frac{\Omega_{m,0}}{1 - \frac{\alpha}{4}} - \Omega_{r,0}\right)a^{\frac{4-4\alpha}{\alpha}} \quad (7) \quad w_{de}(a) = \frac{\alpha-4}{3\alpha\left(1 - \frac{\alpha\Omega_{m,0}}{(\alpha-4)(1-\Omega_{r,0})+4\Omega_{m,0}}a^{\frac{\alpha-4}{\alpha}}\right)}$$

$$(8) \quad \left\{ \begin{array}{l} \frac{\delta P_{de}}{\bar{\rho}_{de}} = \hat{c}_s^2 \delta + \frac{3aH(\hat{c}_s^2 - c_a^2)}{k^2} V \\ \delta' = -\frac{V}{Ha^2} \left(1 + \frac{9a^2 H^2 (\hat{c}_s^2 - w_{de})}{k^2} + \frac{3a^3 H^2 w'_{de}}{k^2(1+w_{de})} \right) - \frac{3}{a} (\hat{c}_s^2 - w_{de}) \delta + 3(1+w_{de}) \phi' \\ V = -\left(1 - 3\hat{c}_s^2 - \frac{aw'_{de}}{(1+w_{de})} \right) \frac{V}{a} + \frac{k^2 \hat{c}_s^2}{Ha^2} \delta + (1+w_{de}) \frac{k^2}{Ha^2} \phi \\ \delta'_m = -\frac{V_m}{Ha^2} + 3\phi' \\ V_m = -\frac{V_m}{a} + \frac{k^2}{Ha^2} \phi \\ k^2 \phi = -4\pi G a^2 \sum_j \rho_j \left(\delta_j + \frac{3aH}{k^2} V_j \right) \end{array} \right.$$

$$E^2(a) = \Omega_{r,0}a^{-4} + \left(1 + \frac{\alpha}{4-\alpha}\right)\Omega_{m,0}a^{-3} + \left(1 - \frac{\Omega_{m,0}}{1 - \frac{\alpha}{4}} - \Omega_{r,0}\right)a^{\frac{4-4\alpha}{\alpha}} \quad (7) \quad w_{de}(a) = \frac{\alpha-4}{3\alpha\left(1 - \frac{\alpha\Omega_{m,0}}{(\alpha-4)(1-\Omega_{r,0})+4\Omega_{m,0}}a^{\frac{\alpha-4}{\alpha}}\right)}$$

$$(8) \quad \left\{ \begin{array}{l} \frac{\delta P_{de}}{\bar{\rho}_{de}} = \hat{c}_s^2 \delta + \frac{3aH(\hat{c}_s^2 - c_a^2)}{k^2} V \\ \delta' = -\frac{V}{Ha^2} \left(1 + \frac{9a^2 H^2 (\hat{c}_s^2 - w_{de})}{k^2} + \frac{3a^3 H^2 w'_{de}}{k^2 (1+w_{de})} \right) - \frac{3}{a} (\hat{c}_s^2 - w_{de}) \delta + 3(1+w_{de}) \phi' \\ V' = -\left(1 - 3\hat{c}_s^2 - \frac{aw'_{de}}{(1+w_{de})} \right) \frac{V}{a} + \frac{k^2 \hat{c}_s^2}{Ha^2} \delta + (1+w_{de}) \frac{k^2}{Ha^2} \phi \\ \delta'_m = -\frac{V_m}{Ha^2} + 3\phi' \\ V'_m = -\frac{V_m}{a} + \frac{k^2}{Ha^2} \phi \\ k^2 \phi = -4\pi G a^2 \sum_j \rho_j \left(\delta_j + \frac{3aH}{k^2} V_j \right) \end{array} \right.$$

$$(9) \quad H^2 = H_0^2 \Omega_{m,0}^{\text{eff}} a^{-3}$$

$$E^2(a) = \Omega_{r,0}a^{-4} + \left(1 + \frac{\alpha}{4-\alpha}\right)\Omega_{m,0}a^{-3} + \left(1 - \frac{\Omega_{m,0}}{1 - \frac{\alpha}{4}} - \Omega_{r,0}\right)a^{\frac{4-4\alpha}{\alpha}} \quad (7) \quad w_{de}(a) = \frac{\alpha-4}{3\alpha\left(1 - \frac{\alpha\Omega_{m,0}}{(\alpha-4)(1-\Omega_{r,0})+4\Omega_{m,0}}a^{\frac{\alpha-4}{\alpha}}\right)}$$

$$(8) \quad \left\{ \begin{array}{l} \frac{\delta P_{de}}{\bar{\rho}_{de}} = \hat{c}_s^2 \delta + \frac{3aH(\hat{c}_s^2 - c_a^2)}{k^2} V \\ \delta' = -\frac{V}{Ha^2} \left(1 + \frac{9a^2 H^2 (\hat{c}_s^2 - w_{de})}{k^2} + \frac{3a^3 H^2 w'_{de}}{k^2 (1+w_{de})} \right) - \frac{3}{a} (\hat{c}_s^2 - w_{de}) \delta + 3(1+w_{de}) \phi' \\ V' = -\left(1 - 3\hat{c}_s^2 - \frac{aw'_{de}}{(1+w_{de})} \right) \frac{V}{a} + \frac{k^2 \hat{c}_s^2}{Ha^2} \delta + (1+w_{de}) \frac{k^2}{Ha^2} \phi \\ \delta'_m = -\frac{V_m}{Ha^2} + 3\phi' \\ V'_m = -\frac{V_m}{a} + \frac{k^2}{Ha^2} \phi \\ k^2 \phi = -4\pi G a^2 \sum_j \rho_j \left(\delta_j + \frac{3aH}{k^2} V_j \right) \end{array} \right.$$

$$(9) \quad H^2 = H_0^2 \Omega_{m,0}^{\text{eff}} a^{-3}$$

$$(10) \quad \left\{ \begin{array}{l} \delta_m = \delta_0 \left(a + 3 \frac{H_0^2 \Omega_{m,0}^{\text{eff}}}{k^2} \right) \\ V_m = -\delta_0 H_0 \sqrt{\Omega_{m,0}^{\text{eff}}} a^{1/2} \\ \delta = \delta_m \\ V = V_m \\ \delta_0 \equiv -\frac{2k^2 \phi_0}{3H_0^2 \Omega_{m,0}^{\text{eff}}} \end{array} \right.$$

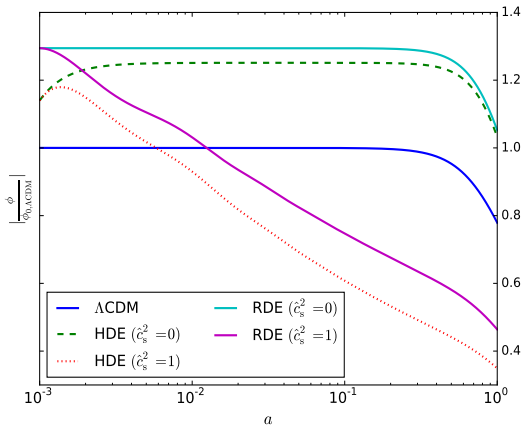


Figure 2: Evolution of the gravitational potential in ΛCDM , HDE, and RDE. $\Omega_{r,0} = 0$, $\Omega_{m,0} = 0.3$, $H_0 = 70 \text{ km s}^{-1} \text{ Mpc}^{-1}$, $k = 25H_0$, $\delta_0 = 1$; for RDE $\alpha = 0.91$; for HDE $\alpha = 0.88$ and $\beta = 0.39$.

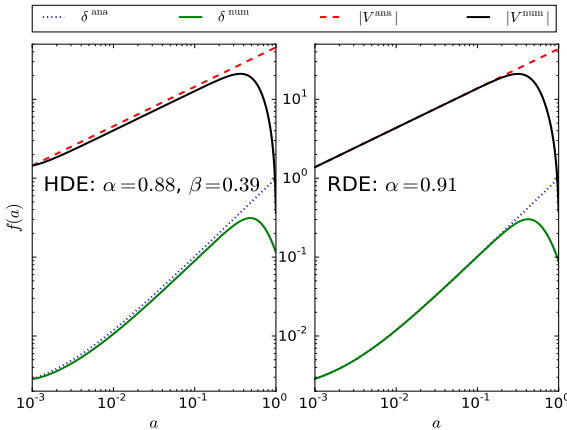


Figure 3: The evolution of DE perturbations in HDE (left panel) and RDE (right panel). Same cosmological parameters.

CLASS

The Cosmic Linear Anisotropy Solving System ^a

-
- ^a Lucca, M., Schöneberg, N., Hooper, D. C., Lesgourgues, J., Chluba, J. (2020). The synergy between CMB spectral distortions and anisotropies. *Journal of Cosmology and Astroparticle Physics*, 2020(02), 026.
<http://class-code.net/>

PPF

Parametrized Post-Friedmann^a

-
- ^a Fang, W., Hu, W., Lewis, A. (2008). Crossing the phantom divide with parametrized post-Friedmann dark energy. *Physical Review D*, 78(8), 087303.

Our Code: EFCLASS



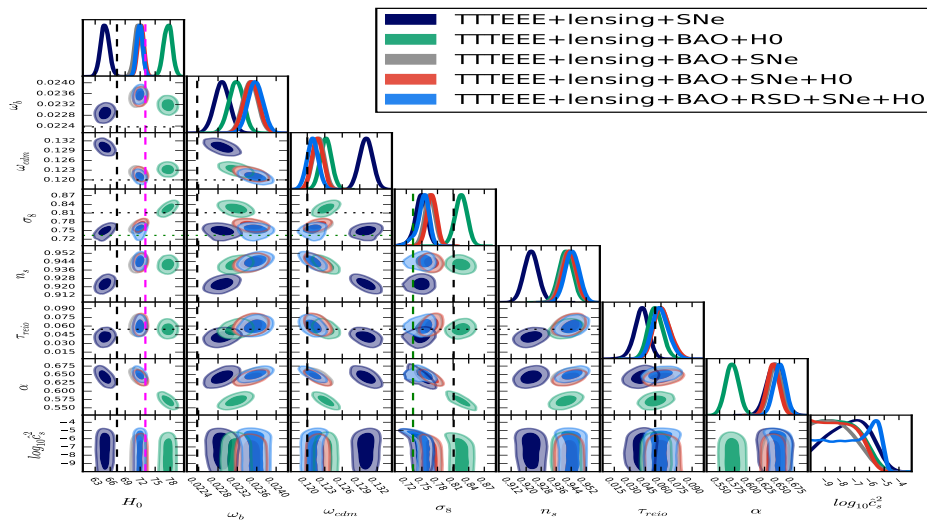


Figure 4: 1D marginalised likelihoods as well as confidence contours (i.e., 68% and 95%) for the RDE cosmological model. Black lines (Planck.), magenta line (SH0ES) and green (DES).

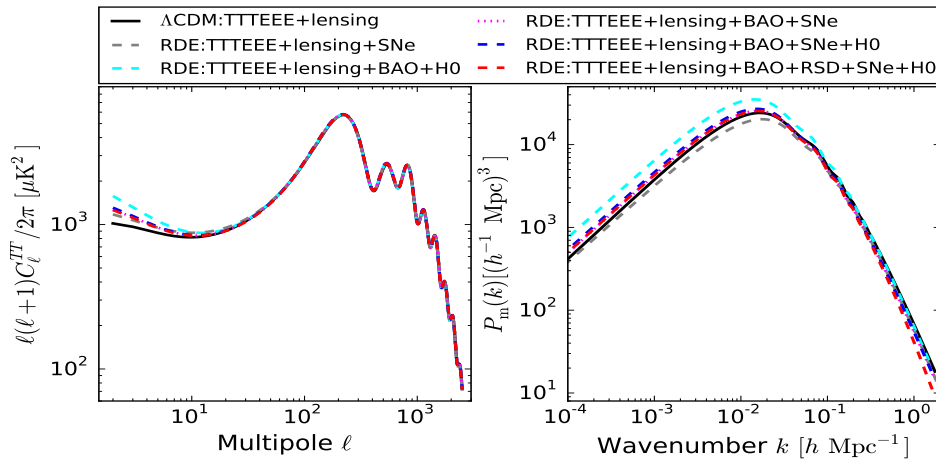


Figure 5: Left: CMB temperature angular power spectrum C_ℓ^{TT} . Right: linear theory matter power spectrum $P_m(k, z = 0)$. Our baseline result (TTTEEE+lensing+BAO+RSD+SNe+H0) has the following best fit values for cosmological parameters: $\omega_b = 0.02351$, $\omega_{\text{cdm}} = 0.1214$, $100\theta_s = 1.04087$, $\ln 10^{10} A_s = 3.014$, $n_s = 0.9440$, $\tau = 0.0551$, $\alpha = 0.651$, $\log \hat{c}_s^2 = -6$, $\sigma_8 = 0.736$, $H_0 = 71.44 \text{ km s}^{-1} \text{ Mpc}^{-1}$.

Some important conclusions

- In the literature, a RDE model with fixed $\hat{c}_s^2 = 1$ has been investigated. Nevertheless, we showed **this choice might not be appropriate** as it heavily affects matter clustering through changes in the gravitational potential during matter dominance.
- Our findings show that matter perturbations behave slightly different with respect to Λ CDM. Due to the matter-like behaviour of the HDE in the RDE model, **DE clusters in the same way as matter perturbations**.
- For our baseline result using all data sets we found that $\hat{c}_s^2 = 1$ is excluded at $\gtrsim 3\sigma$. We also obtained a value of σ_8 lower than in the model and in good agreement ($\approx 2\sigma$) with recent DES results. Finally, our constraint on the H_0 value is also in good concordance ($\approx 2\sigma$) with local, model independent measurements using Cepheid variables.
- Our work shows that **dynamical DE also having non standard clustering properties** might play a part in the solution of discrepancies in cosmological parameters.



Thanks!!

If ρ is the quantum zero-point energy density associated to a UV cut-off, the total energy in a region of size L should not exceed the mass of a black hole of the same size, namely,

$$L^3 \rho \leq L M_p^2, \quad (1)$$

where M_p is the reduced Planck mass. The largest, allowed IR cut-off L_{IR} saturates the inequality (??) so that the maximum energy density in the effective theory is given by

$$\rho = 3\gamma^2 M_p^2 L_{\text{IR}}^{-2}, \quad (2)$$

We assume a flat, linearly perturbed Friedmann-Lemaître-Robertson-Walker metric (FLRW). In the conformal Newtonian gauge form *P. Ma and E. Bertschinger* *The Astrophysical Journal* 455 (1995)

$$ds^2 = a(\tau)^2 \left[-(1 + 2\psi(\vec{x}, \tau))d\tau^2 + (1 - 2\phi(\vec{x}, \tau))d\vec{x}^2 \right], \quad (3)$$

where $a(\tau)$ is the scale factor, and ψ, ϕ denote the gravitational potentials.

The effective parameter densities satisfy $\Omega_{m,0}^{\text{eff}} + \Omega_{r,0}^{\text{eff}} + \Omega_{de,0}^{\text{eff}} = 1$. Note that the HDE parameter density reads

$$\Omega_{de} = \left(\frac{\alpha - 2\beta}{1 - \alpha + 2\beta} \right) \Omega_{r,0} a^{-4} + \left(\frac{2\alpha - 3\beta}{2 - 2\alpha + 3\beta} \right) \Omega_{m,0} a^{-3} + \Omega_{de,0}^{\text{eff}} a^{\frac{-2(\alpha-1)}{\beta}}$$

$$w_{de}(a) = \frac{\left(\frac{2\alpha - 3\beta - 2}{3\beta} \right) \Omega_{de,0}^{\text{eff}} a^{\frac{-2(\alpha-1)}{\beta}} + \left(\frac{2\beta - \alpha}{3\alpha - 6\beta - 3} \right) \Omega_{r,0} a^{-4}}{\left(\frac{2\alpha - 3\beta}{2 - 2\alpha + 3\beta} \right) \Omega_{m,0} a^{-3} + \left(\frac{\alpha - 2\beta}{1 - \alpha + 2\beta} \right) \Omega_{r,0} a^{-4} + \Omega_{de,0}^{\text{eff}} a^{\frac{-2(\alpha-1)}{\beta}}}$$

for RDE

$$c_a^2 \equiv \frac{dP_{de}}{d\rho_{de}} = w_{de} - \frac{w'_{de}}{3H(1+w_{de})} = w_{de} - \frac{w'_{de}a}{3(1+w_{de})}$$

$$= \frac{4(\alpha - 4)}{3\alpha \left(4 - \frac{3\alpha^2 \Omega_{m,0}}{(\alpha-1)((\alpha-4)(1-\Omega_{r,0})+4\Omega_{m,0})} a^{\frac{\alpha-4}{\alpha}} \right)} \quad (4)$$

The linearised Einstein field equations

$$k^2 \phi + 3 \frac{\dot{a}}{a} \left(\dot{\phi} + \frac{\dot{a}}{a} \psi \right) = 4\pi G a^2 \delta T_0^0, \quad (5)$$

$$k^2 \left(\dot{\phi} + \frac{\dot{a}}{a} \psi \right) = 4\pi G a^2 (\bar{\rho}_{\text{fld}} + \bar{P}_{\text{fld}}) \theta_{\text{fld}}, \quad (6)$$

$$\ddot{\phi} + \frac{\dot{a}}{a} (\dot{\psi} + 2\dot{\phi}) + \left(2\frac{\ddot{a}}{a} - \frac{\dot{a}^2}{a^2} \right) \psi + \frac{k^2}{3} (\phi - \psi) = \frac{4\pi}{3} G a^2 \delta T_i^i, \quad (7)$$

$$k^2 (\phi - \psi) = 12\pi G a^2 (\bar{\rho}_{\text{fld}} + \bar{P}_{\text{fld}}) \sigma_{\text{fld}}, \quad (8)$$

where k is the wavenumber, the divergence of the velocity field is defined as $\theta_{\text{fld}} \equiv ik^j u_j$, and σ_{fld} is the anisotropic stress. From the conservation of energy-momentum ($\nabla_\mu T^{\mu\nu} = 0$) for a single fluid we obtain

$$\dot{\delta}_{\text{fld}} = -V_{\text{fld}} + 3(1 + w_{\text{fld}})\dot{\phi} - 3 \frac{\dot{a}}{a} \left(\frac{\delta P_{\text{fld}}}{\bar{\rho}_{\text{fld}}} - w_{\text{fld}} \delta_{\text{fld}} \right), \quad (9)$$

$$\dot{V}_{\text{fld}} = -\frac{\dot{a}}{a} (1 - 3w_{\text{fld}}) V_{\text{fld}} + \frac{\delta P_{\text{fld}}}{\bar{\rho}_{\text{fld}}} k^2 + k^2 (1 + w_{\text{fld}}) \phi, \quad (10)$$

where we have used the scalar velocity perturbation $V_{\text{fld}} \equiv ik_j T_0^j / \bar{\rho} = (1 + w_{\text{fld}}) \theta_{\text{fld}}$ and disregarded anisotropic stress.

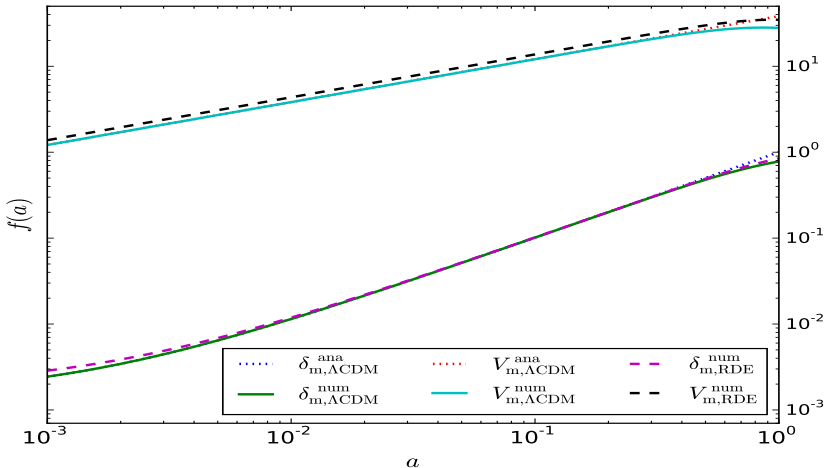


Figure 6: Evolution of density and velocity matter perturbations in the Λ -CDM and RDE ($\hat{c}_s^2 = 0$) model. We show the numerical solutions (solid and dashed curves) as well as the analytical solutions (dotted curves) in MD for the standard cosmological model.

The PPF description of DE replaces the density and momentum components with a single joint dynamical variable

$$\Gamma \equiv -\frac{4\pi G a^2}{k^2 c_K} \delta \hat{\rho}_{de}, \quad (11)$$

thus reducing closure conditions, but requiring strict conservation of energy and momentum in its equation of motion. Here $c_K = 1 - 3K/k^2$, where K is the space-time curvature that we set to $K = 0$. The evolution equation for Γ is given by

$$(1 + c_\Gamma^2 k_H^2) \left[\frac{\dot{\Gamma}}{H} + \Gamma + c_\Gamma^2 k_H^2 \Gamma \right] = S, \quad (12)$$

where $c_\Gamma \equiv 0.4 \hat{c}_s$ calibrates the scale of the transition, $k_H = k^2/aH$ and

$$S = \frac{\dot{a}}{a} \frac{4\pi G}{H^2} \rho_{de} (1+) \frac{\theta_T}{k^2} \quad (13)$$

where the subscript T denotes all species except dark energy.

Data constraining we uses:

- Baryon Acoustic Oscillations (BAO)¹
- Pantheon supernovae (SNe)²
- SH0ES local measurement of the Hubble constant (H_0)³, that we introduce as a Gaussian prior.
- CMB lensing (lensing) as well as temperature and polarisation anisotropies of the CMB (TTTEEE) measured by the Planck Collaboration⁴
- Compilation of Redshift-Space-Distortions RSD⁵.

¹BOSS collaboration, The clustering of galaxies in the completed SDSS-III Baryon Oscillation Spectroscopic Survey: cosmological analysis of the DR12 galaxy sample, Mon. Not. Roy. Astron. Soc. 470 (2017) 2617

²Pan-STARRS1 collaboration, The Complete Light-curve Sample of Spectroscopically Confirmed SNe Ia from Pan-STARRS1 and Cosmological Constraints from the Combined Pantheon Sample, Astrophys. J. 859 (2018) 101

³A. G. Riess et al., A Comprehensive Measurement of the Local Value of the Hubble Constant with 1 km s⁻¹ Mpc⁻¹ Uncertainty from the Hubble Space Telescope and the SH0ES Team, Astrophys. J. Lett. 934 (2022) L7

⁴Planck collaboration, Planck 2018 results. VI. Cosmological parameters, Astron. Astrophys. 641 (2020) A6

⁵R. Arjona, J. García-Bellido and S. Nesseris, Cosmological constraints on nonadiabatic dark energy perturbations, Phys. Rev. D 102 (2020) 103526

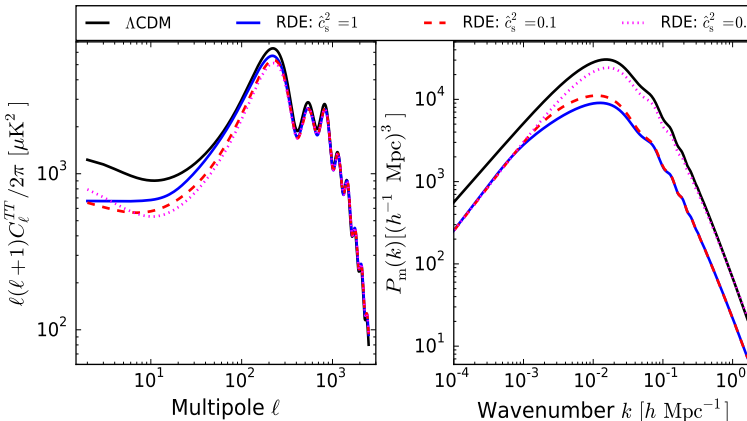


Figure 7: CMB temperature angular power spectrum C_l^{TT} and matter power spectrum $P(k, z = 0)$ for different values of \hat{c}_s^2 . $\alpha = 0.6904$ (note that authors in Ref.⁶ actually report $\beta = 0.3452$).

⁶Y. Wang, L. Xu and Y. Gui, Probing Ricci dark energy model with perturbations by using WMAP seven-year cosmic microwave background measurements, BAO and Type Ia supernovae, Phys. Rev. D 84 (2011)

Constraining the background

| Parameter | HDE:BAO | HDE:BAO+SNe | HDE:BAO+SNe+H0 | RDE:BAO+SNe+H0 |
|-----------------------|------------------------------|------------------------------|------------------------------|------------------------------|
| ω_b | $0.0195_{-0.0144}^{+0.0051}$ | $0.0151_{-0.0097}^{+0.0025}$ | $0.0176_{-0.0108}^{+0.0039}$ | $0.0228_{-0.0106}^{+0.0048}$ |
| ω_{cdm} | $0.0688_{-0.0585}^{+0.0334}$ | $0.0821_{-0.0261}^{+0.0363}$ | $0.1010_{-0.0319}^{+0.0384}$ | $0.1202_{-0.0292}^{+0.0408}$ |
| β | $0.49_{-0.13}^{+0.08}$ | $0.43_{-0.08}^{+0.04}$ | $0.40_{-0.08}^{+0.06}$ | — |
| α | $1.14_{-0.18}^{+0.22}$ | $0.98_{-0.13}^{+0.10}$ | $0.95_{-0.11}^{+0.10}$ | $0.92_{-0.13}^{+0.10}$ |
| $\Omega_{\text{m},0}$ | $0.195_{-0.091}^{+0.077}$ | $0.214_{-0.054}^{+0.063}$ | $0.222_{-0.054}^{+0.062}$ | $0.268_{-0.045}^{+0.056}$ |

Table 1: Mean values and 68% confidence limits on cosmological parameters. Here we only use data constraining the background.

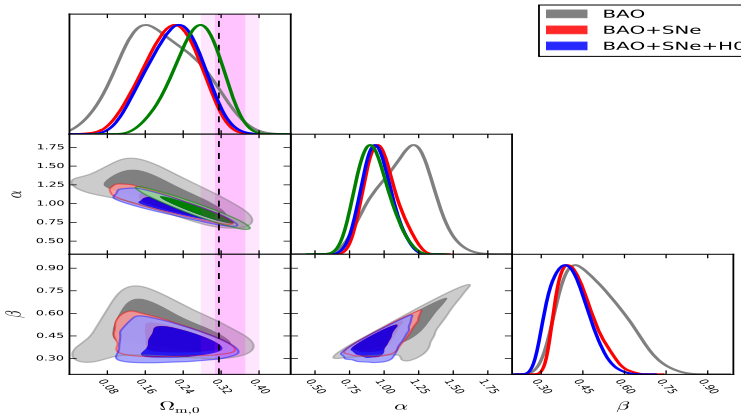


Figure 8: 1D marginalised likelihoods as well as confidence contours (i.e., 68% and 95%) for the HDE (i.e., gray, red, and blue) cosmological model. Green contours and curves show results for the RDE model with BAO+SNe+H0. Note that here we plot the matter density parameter $\Omega_{m,0} \equiv (\omega_b + \omega_{cdm})/h^2$ which is a derived parameter in our analysis. Dashed, vertical line indicates the result obtained by the Planck Collaboration using the standard cosmological model(Planck 2018 results. VI) Vertical bands indicate DES (Year 3) results (68% and 95% confidence intervals) for Λ -CDM.

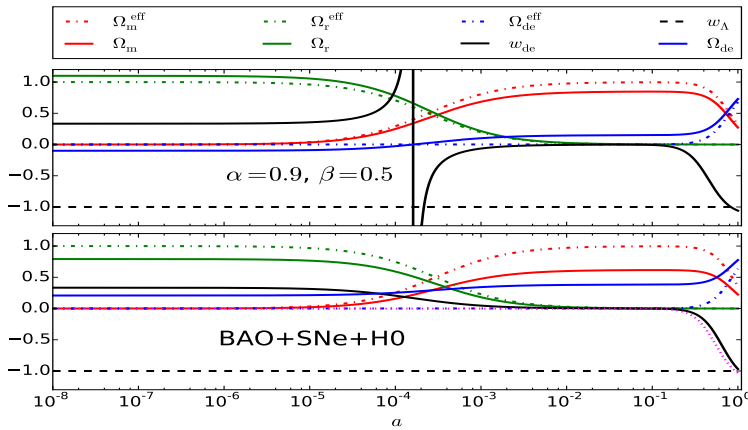


Figure 9: Evolution of parameter densities and HDE equation of state for the HDE model. In the lower panel we use the best fit values for HDE:BAO+SNe+H0 ($\alpha = 0.906$, $\beta = 0.349$, $H_0 = 72.90 \text{ km s}^{-1} \text{ Mpc}^{-1}$, $\Omega_{m,0} = 0.224$). The magenta, dotted curve shows for the best fit of RDE:BAO+SNe+H0 ($\alpha = 0.893$, $H_0 = 73.12 \text{ km s}^{-1} \text{ Mpc}^{-1}$, $\Omega_{m,0} = 0.281$). We set $\Omega_{r,0} = 8.5 \times 10^{-5}$, and for the upper panel we use $\Omega_{m,0} = 0.2713$.

| Parameter | TTTEEE+lensing+SNe | {...}+BAO | {...}+H0 | {...}+RSD | TTTEEE+lensing+BAO+H0 |
|-----------------------|---------------------------------|------------------------------|------------------------------|------------------------------|------------------------------|
| ω_b | $0.02288^{-0.00015}_{+0.00016}$ | 0.02347 ± 0.00015 | 0.02349 ± 0.00015 | 0.02357 ± 0.00015 | 0.02317 ± 0.00015 |
| ω_{cdm} | 0.1301 ± 0.0011 | 0.1219 ± 0.0010 | 0.1218 ± 0.0010 | 0.1209 ± 0.0010 | $0.1232^{-0.0010}_{+0.0009}$ |
| H_0 | $64.95^{-0.83}_{+0.84}$ | $71.65^{-0.73}_{+0.75}$ | $72.12^{-0.62}_{+0.60}$ | $71.91^{-0.61}_{+0.59}$ | $77.55^{-0.85}_{+0.82}$ |
| σ_8 | $0.748^{-0.010}_{+0.013}$ | 0.765 ± 0.010 | 0.769 ± 0.009 | $0.752^{-0.008}_{+0.014}$ | 0.825 ± 0.012 |
| n_s | 0.9226 ± 0.0038 | 0.9425 ± 0.0038 | 0.9431 ± 0.0037 | $0.9445^{-0.0037}_{+0.0038}$ | 0.9412 ± 0.0037 |
| τ | $0.0411^{-0.0061}_{+0.0071}$ | $0.0605^{-0.0085}_{+0.0072}$ | $0.0612^{-0.0090}_{+0.0070}$ | $0.0596^{-0.0086}_{+0.0070}$ | $0.0547^{-0.0073}_{+0.0065}$ |
| log | -7^{-2}_{+1} | < -8 | < -7 | < -6 | -8^{-2}_{+1} |
| α | 0.642 ± 0.013 | 0.643 ± 0.011 | 0.640 ± 0.010 | 0.650 ± 0.010 | 0.571 ± 0.011 |
| $\Omega_{\text{m},0}$ | 0.363 ± 0.011 | $0.283^{-0.007}_{+0.006}$ | $0.279^{-0.006}_{+0.005}$ | 0.279 ± 0.005 | $0.243^{-0.005}_{+0.006}$ |
| $100\theta_\star$ | 1.03999 ± 0.00028 | 1.04084 ± 0.00028 | 1.04088 ± 0.00028 | 1.04092 ± 0.00028 | 1.04076 ± 0.00028 |
| S_8 | $0.822^{-0.012}_{+0.014}$ | 0.744 ± 0.010 | 0.742 ± 0.010 | $0.726^{-0.010}_{+0.014}$ | 0.743 ± 0.010 |

Table 2: Mean values and 68% confidence limits on cosmological parameters for the RDE model. Here {...} stands for the inclusion of data from column on the left.

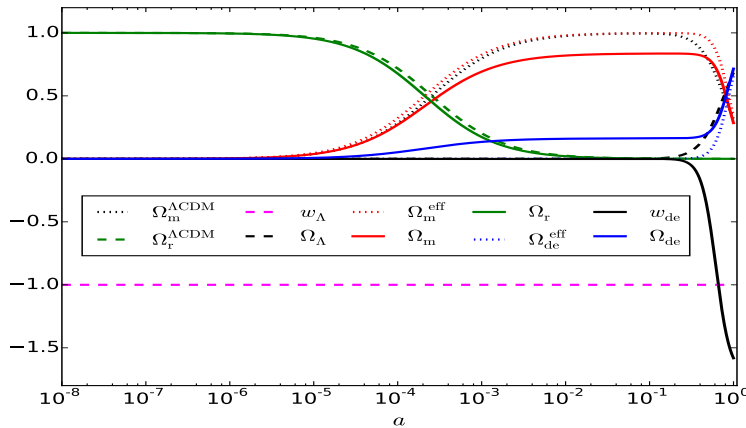


Figure 10: Evolution of parameter densities and DE equation of state for the RDE model. Here we use the best fit values for our baseline result (TTTEEE+lensing+BAO+RSD+SNe+H0). For sake of comparison we also plot the Λ -CDM baseline result by the Planck Collaboration.

For the Λ -CDM Planck baseline

$$100\theta_s = 1.04110, \quad r_s(z_*) = 144.531055 \text{ Mpc}, \quad d_A(z_*) = 12.738778 \text{ Mpc}, \quad (14)$$

our baseline result (the best fit)

$$100\theta_s = 1.04087, \quad r_s(z_*) = 136.800000 \text{ Mpc}, \quad d_A(z_*) = 12.053113 \text{ Mpc}, \quad (15)$$

The RDE model decreases both the sound horizon and the comoving angular diameter distance while keeping the angular acoustic scale in good agreement with the Λ -CDM solution.

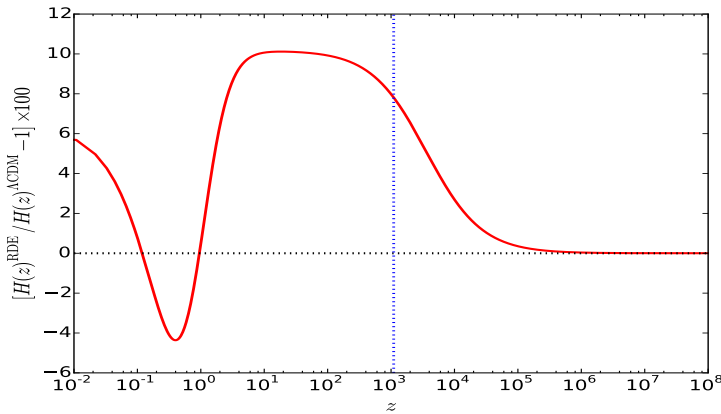


Figure 11: Percentage difference in the Hubble parameter for the RDE model (best fit of our baseline result) with respect to the Planck. Blue, vertical dotted line indicates z_* .

The RDE model the expansion rate is enhanced with respect to the standard model in two stages ($10^0 \lesssim z \lesssim 10^5$ and at late times $z \lesssim 10^{-1}$). On the other hand, the universe expands faster in Λ -CDM than in RDE for $10^{-1} \lesssim z \lesssim 10^0$.

MCMC

We performed a Markov Chain Monte Carlo (MCMC) statistical analysis by sampling the parameter space with the code Monte Python. The latter is linked to CLASS and samples the parameter space with the default Metropolis-Hastings algorithm.

- In a first stage, a covariance matrix is adjusted so that the acceptance rate is ≈ 0.25 .
- In a second stage of the analysis, the covariance matrix is fixed and the code performs $\sim 10^6$ iterations until reaching convergence which we estimate with the Gelman-Rubin statistic R satisfying the condition $R - 1 \lesssim 0.01$ for all the varying parameters.

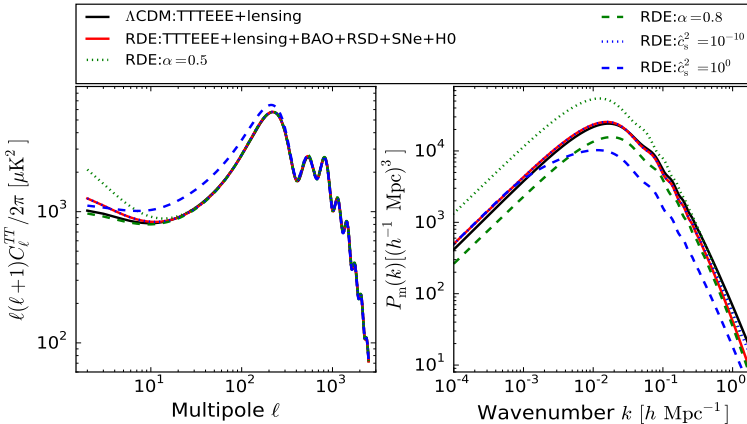


Figure 12: Left: CMB angular power spectrum. Right: linear theory matter power spectrum. Solid, black lines show the Planck Collaboration baseline result for the standard model. Solid, red lines show our baseline result for the RDE model. Green, dotted (dashed) line shows the effect of decreasing (increasing) α with respect to the best fit value. Blue, dotted (dashed) line shows the effect of decreasing (increasing) \hat{c}_s^2 with respect to the best fit value.

Others conclusions

- In previous works radiation is not properly taken into account when solving for the Hubble parameter. We showed this might not be a good approximation: depending on the cut-off choice, new terms might appear playing a part in early stages of the universe expansion.
- The RDE cosmological model can decrease both sound horizon and comoving angular diameter distance while keeping good agreement with CMB measurements of the angular acoustic scale. This feature might help to relax the current discrepancy in the Hubble constant between low and high redshift probes.